Computational model for multifocal imaging in optical projection tomography and numerical analysis of all-in-focus fusion in tomographic image reconstruction

O. Koskela[1], S. Pursiainen[2], B. Belay[1], T. Montonen[1], E. Figueiras[3] and J. Hyttinen[1]

[1] BioMediTech Institute and Faculty of Biomedical Sciences and Engineering, Tampere University of Technology, Tampere, Finland
[2] Department of Mathematics, Tampere University of Technology, Tampere, Finland
[3] Ultrafast Bio- and Nano-photonics Group, International Iberian Nanotechnology Laboratory, Braga, Portugal

Abstract— **Optical projection tomography (OPT) is a non-invasive 3D imaging method that has been used to study small biological samples. In OPT samples can be mounted in hydrogel scaffold mimicking real life extracellular matrix, and hence grown in all natural dimensions. In optical imaging systems, focusing lenses are required for image acquisition. Due to these lenses, particles at a certain distance from objectives — in the focal plane of the lens — are captured accurately and the further a particle is from the focal plane the blurrier it is captured in the resulting image. To compensate this limitation, multifocal OPT is implemented, where images from each angle are taken with multiple focal planes at different distances. From these images, parts in focus are detected and combined into a single image using all-in-focus fusion algorithm. In this work we present computational way of modeling multifocal imaging and use the presented model to assess the performance of two different all-in-focus fusion methods.**

Keywords— **optical projection tomography, tomographic image reconstruction, all-in-focus fusion, multifocal microscopy, optical 3D microscopy**

I. Introduction

Optical projection tomography (OPT) is a non-invasive three-dimensional microscopy method that can image mesoscopic samples of diameter 1–10 mm in real life mimicking hydrogel scaffold [1]. It has been applied in time lapse imaging of biological samples in the field of developmental biology [2]. Recently it has been shown to be a prominent tool to study mass transport in and characterize different types of hydrogels [3]. OPT's advantages are its sample size range and possibility to image in living organisms in non-harmful way.

In optical imaging out-of-focus blurring of particles is dependent on their distance to the focal plane of the imaging system. Particles at the focal plane are captured accurately and the further a particle is from focal plane the blurrier it is in the resulting image. Blurring is also varying with numerical aperture of the focusing lens system. Using a high numerical aperture lens higher resolution at the focal plane is gained with the expense of even blurrier particles as the depth of (focal) field is shorter.

Standard OPT systems have numerical aperture reduced to cover half of the sample within the depth of field [1]. Recent technical development of OPT such as development of dual-axis OPT [4], focal scanning through the sample using lead zirconate titanate (PZT) scanner [5] or helical sample rotation trajectory [2], and electrically tunable lens integrated to OPT for multi-focal imaging [5, 6] allowed to extend the depth of field of OPT imaging system.

In multifocal imaging multiple projections with different focal distances from each projection angle are acquired and fused into single all-in-focus image. All-in-focus fusion methods have been studied as a computer vision problem [7, 8], but so far it remains unclear, how to choose a suitable all-in-focus method and what errors and artifact such a choice pronounces.

In this work we include a simple step in the simulated OPT forward projection procedure to model a focusing lens system and with this adjustment, we study numerically the effect of multifocal imaging and all-in-focus fusion into the yielding reconstructions.

II. Materials and methods

A. Forward model

Standard Radon transform in tomography under parallel beam geometry consists of ray-transform in y direction through applying Beer-Lambert law to the numerical phantom $P \in \mathbf{R}^3$. This assumes everything within the sample to be equally and absolutely focused. Point spread function and possible noise of the detection is applied to simulated data afterward.

Focal plane can be defined as a two dimensional plane perpendicular to x and z coordinates in $\mathbf{R}$. Note here that focal plane is always orthogonal to ray-transform. In this setting, we model optical detection through a convolution in x and z coordinates of the phantom and a focusing kernel matrix F in

each rotational position before ray-transform. Matrix $F \in \mathbf{R}^2$ describes the focusing properties the lens.

In this study we assume that focusing can be modeled as a Gaussian phenomena. An x-axisymmetric bounding function $y \mapsto f(y)$ tells the width of the kernel with respect to y and follows a Gaussian curvature. For each depth y, $F(x,y)$ is again Gaussian along x and its deviation increases as a function of distance to focal depth.

In other words: for each pixel in the detector at $(x_i, y_i, z_i) \in \mathbf{R}$, align center of F to the coordinates x_i and z_i (separately in both dimensions), and compute the values of the phantom weighted with the values of the focusing kernel F. Hence the values in F can also be thought as the contribution weights of phantom pixels in a single ray.

Figures 1a and 1c shows the two chosen focusing kernels in this study. The focal model is sharpest at the focal plane and from there the convolution kernel gradually widens in horizontal direction.

B. All-in-fusion algorithms

In this comparison we use two all-in-focus fusion algorithms, namely extended depth of field (eDOF) from [2] and Stack Focuser [9].

eDOF is computational and memory efficient algorithm as it can sum up the projection images as they come and then discard it from memory. Given N images I_i all with different focal regions, the all-in-focus fusion I^E can be expressed as

$$I^E = \frac{\sum_{i=1}^{N} I_i \cdot \left| I_i^{HP} \right|}{\sum_{i=1}^{N} \left| I_i^{\mathrm{HP}} \right|}. \tag{1}$$

I_i^{HP} is the high pass replica of the i^{th} image. Computation of high pass replica was implemented as $I_i^{\mathrm{HP}} = I_i - I_i^{\mathrm{LP}}$ where LP refers to low pass filtered image, a moving window average filtered image.

Stack Focuser is an ImageJ plugin that was re-implemented in MATLAB by the authors. The algorithm has the following steps: 1) create a copy of the image stack, 2) median filter the copy with 3×3 median filter and then Sobel filter to find the edges, 3) create a height map: for each pixel in the copy take the maximum value of its neighborhood of specified size, and 4) for each pixel in the resulting (2D) image find the maximum value in the third dimension of the height map and take corresponding pixel value from the original (2+1D) image stack.

Stack Focuser is a bit more complex algorithm with more steps in edge detection, and thus requires more computational time and memory allocation.

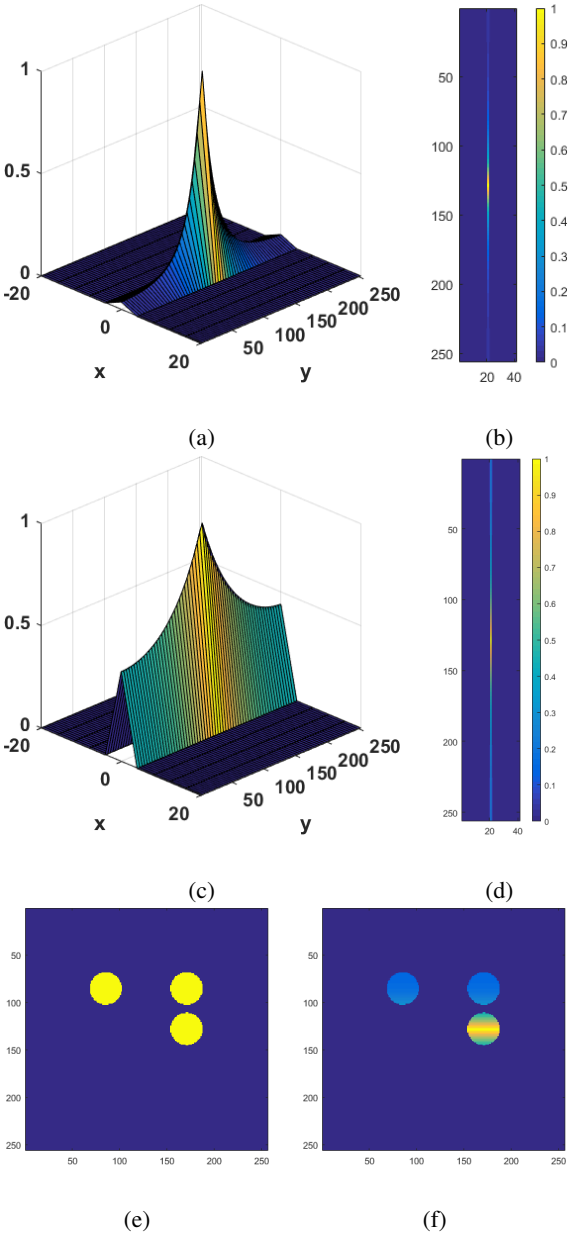

Fig. 1: a) 3D view on the short focal depth focusing kernel: the peak value is at focal plane and from there the intensity decreases and blurring increases. b) Focusing kernel viewed from the top. c) 3D view on the focusing kernel with long focal depth. d) Focusing kernel viewed from the top. e) The phantom used in this study and f) the effect of horizontal row-wise convolution.

C. Simulations

In this study we simulated projection data from a phantom that was of size $256 \times 256 \times 51$. The slice in reconstructions is represented in Figure 1e. OPT data was simulated with 1 degree intervals and full 360 degrees rotation. Six depth of field schemes were used: without focal plane model for comparison (0FP), then focal plane setup with both long (1FP/L) and short (1FP/S) focal depth systems, and with short focal depth system multifocal imaging with 5, 11, and 21 different focal planes (5FP, 11FP and 21FP). The one focal plane was set to pixel distance 128. Multiple focal planes were equally spaced between [39,205], [13,230], and [1,256] respectively.

In all-in-focus fusion algorithms 4-by-4 window was used for moving average filter kernel size in eDOF and neighborhood size in Stack Focuser. Simulated -20 dB Gaussian distributed noise was added to projection data. All of the computations were performed in MATLAB. Tomographic reconstructions using SIRT and FBP methods were computed using ASTRA tomography toolbox [10] in parallel beam 2D geometry. SIRT was computed using 90 equally distributed projection angles in 360 degrees, and also with all 360 projection angles (referred later as SIRT360).

III. Results

An example of multifocal imaging is shown in Figure 2 presenting five projections from one angle, all-in-focus fusions, projection using longer depth of field, and projection without focusing model. It is apparent that in multifocal projections (Figure 2a) there is more detail available in the data of the particle in left side than in the single focal plane projection (Figures 2e). These details translate differently into all-in-focus fusions in Figures 2b and 2c.

Table 1 summarize the results of simulations in terms of the 2-norm of the difference between reconstruction and original phantom slices. Noticeable is how iterative SIRT performs worse with eDOF than FBP reconstruction, but better when using Stack Focuser. Also when Stack Focuser is used, additional focal planes do not give any enhancement to reconstructions.

Figure 3 illustrates the reconstructions between studied reconstruction methods, number of focal planes and all-in-focus fusion algorithms. The benefit of multifocal imaging can be clearly seen if only a short focal depth system is used. The reconstructions using data from only one focal plane in short focal depth system (1FP/S) are heavily distorted, but using multifocal data the particles in the phantom are reconstructed. Also different behavior between eDOF and Stack Focuser can be noticed, the latter having more pronounced

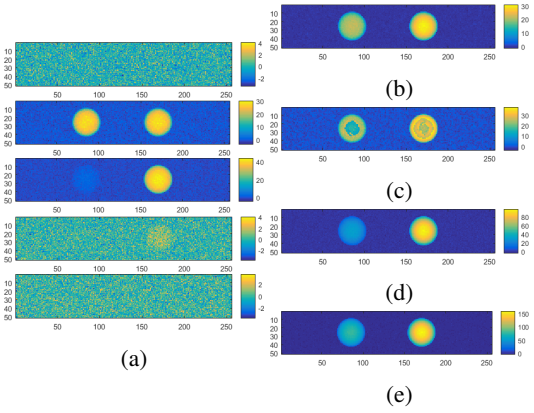

Fig. 2: a) View from one angle of the sample using 5FP. All-in-focus fusions from projections above with b)eDOF and c) Stack Focuser used in this study. d) Simulated view of a single focusing lens (1FP/L) and e) ideal setup with everything in focus for comparison (0FP).

Table 1: Error 2-norms of reconstructions from noisy and noiseless data using FBP with 360 projections angles and SIRT with 90 (referred as SIRT) and 360 (referred as SIRT360) projection angles, both in full angle detection.

	Noiseless		Noisy		
	FBP	SIRT	FBP	SIRT	SIRT360
0FP	45.771	45.786	45.800	45.808	45.799
1FP/L	45.853	45.863	45.861	45.871	45.863
1FP/S	46.304	46.308	46.349	46.349	46.350
eDOF					
5FP	45.742	45.756	45.768	45.782	45.770
11FP	45.653	45.671	45.684	45.701	45.689
21FP	45.602	45.621	45.623	45.641	45.628
Stack Focuser					
5FP	45.831	45.860	45.855	45.885	45.688
11FP	45.831	45.860	45.855	45.885	45.688
21FP	45.831	45.860	45.855	45.885	45.688

edges but centers of particles clearly wrong.

Comparison with the chosen long and short focal depth systems does not clearly indicate in this case, whether more details in all-in-focus fusion projections would actually yield better tomographic reconstruction.

IV. Conclusion

We have presented a forward model for studying OPT and used it to show different behavior of two distinct all-in-focus fusion algorithms in the reconstructions. Both algorithms showed more detail in the all-in-focus fused pro-

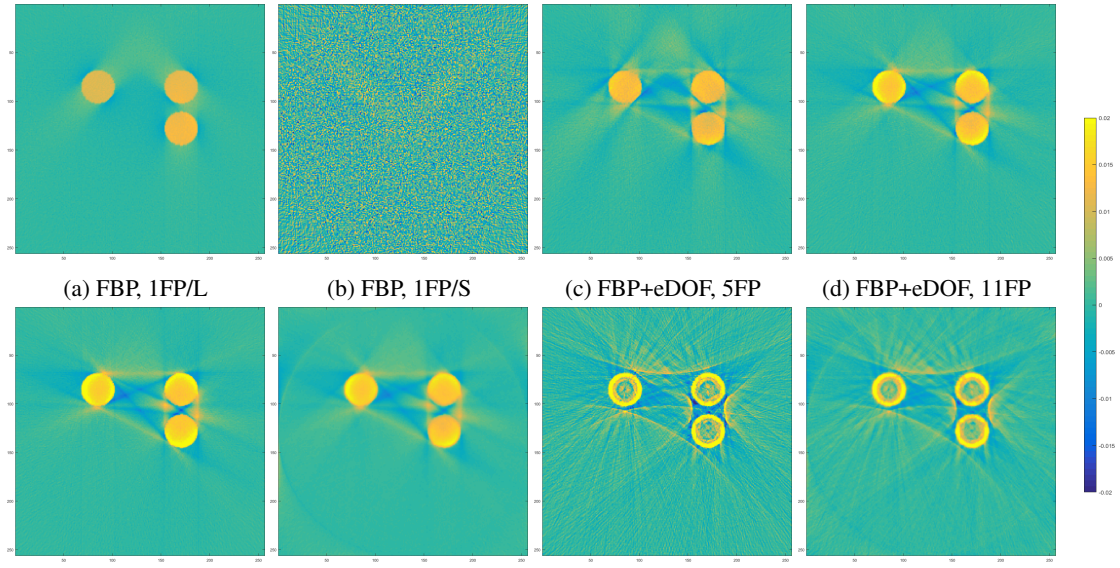

(a) FBP, 1FP/L (b) FBP, 1FP/S (c) FBP+eDOF, 5FP (d) FBP+eDOF, 11FP

(e) FBP+eDOF, 21FP (f) SIRT+eDOF, 11FP (g) FBP+SF, 11FP (h) SIRT+SF, 11FP

Fig. 3: a) FBP reconstruction from the longer focal depth imaging system (1FP/L). b) FBP reconstruction with single focal plane in the short focal depth system (1FP/S). c-e) FBP reconstruction with eDOF fusion and 5, 11, and 21 focal planes respectively. f) SIRT reconstruction with eDOF fusion and 11 focal planes. g) FBP and h) SIRT reconstruction with Stack Focuser fusion and 11 focal planes.

jection images, yet resulted more artifacts in reconstructions than the system with longer focal depth. In author's view the results imply that multifocal imaging and all-in-focus algorithms cannot be used as a plug-and-play technique but a rather deliberate theoretical and practical analysis is required.

Acknowledgements

This work is funded by Jane and Aatos Erkko foundation and Tekes Human Spare Parts program. O. Koskela has received an EXTREMA Cost action grant for ASTRA tomography toolbox training. S. Pursiainen was supported by Academy of Finland Key Project 305055 and Academy of Finland Center of Excellence in Inverse Problems.

Conflicst of interest

The authors declare that they have no conflicts of interest.

References

1. Sharpe James, Ahlgren Ulf, Perry Paul, et al. Optical projection tomography as a tool for 3D microscopy and gene expression studies *Science.* 2002;296:541–545.
2. Bassi Andrea, Schmid Benjamin, Huisken Jan. Optical tomography complements light sheet microscopy for in toto imaging of zebrafish development *Development.* 2015;142:1016–1020.
3. Soto Ana M, Koivisto Janne T, Parraga Jenny E, et al. Optical projection tomography technique for image texture and mass transport studies in hydrogels based on gellan gum *Langmuir.* 2016;32:5173–5182.
4. Chen Lingling, Andrews Natalie, Kumar Sunil, Frankel Paul, McGinty James, French Paul MW. Simultaneous angular multiplexing optical projection tomography at shifted focal planes *Opt. Lett..* 2013;38:851–853.
5. Miao Qin, Hayenga Jon, Meyer Michael G, Neumann Thomas, Nelson Alan C, Seibel Eric J. Resolution improvement in optical projection tomography by the focal scanning method *Opt. Lett..* 2010;35:3363–3365.
6. Chen Lingling, Kumar Sunil, Kelly Douglas, et al. Remote focal scanning optical projection tomography with an electrically tunable lens *Biomed. Opt. Express.* 2014;5:3367–3375.
7. Pertuz Said, Puig Domenec, Garcia Miguel Angel, Fusiello Andrea. Generation of all-in-focus images by noise-robust selective fusion of limited depth-of-field images *IEEE Trans. Image Process..* 2013;22:1242–1251.
8. Li Shutao, Kang Xudong, Fang Leyuan, Hu Jianwen, Yin Haitao. Pixel-level image fusion: A survey of the state of the art *Information Fusion.* 2017;33:100–112.
9. Umorin Michael. Stack Focuser https://imagej.nih.gov/ij/plugins/-stack-focuser.html. Last fetched Feb 8, 2017.
10. van Aarle Wim, Palenstijn Willem Jan, De Beenhouwer Jan, et al. The ASTRA Toolbox: A platform for advanced algorithm development in electron tomography *Ultramicroscopy.* 2015.

Author: Olli Koskela
Institute: BioMediTech Institute and Faculty of Biomedical Sciences and Engineering
Street: Korkeakoulunkatu 10
City: 33720 Tampere
Country: Finland
Email: olli.koskela@tut.fi